Supplementary information

Evidence of solvent-mediated proton transfer during H_2O_2 activation in titanosilicate-catalyzed oxidation systems

Yunkai Yu,[a,c] Jianhao Wang,[a] Nan Fang,[a] Zhen Chen,[a] Dongxu Liu,[a] Yueming Liu,[a,b,*] and Mingyuan He[a,b]

[a] *Shanghai Key Laboratory of Green Chemistry and Chemical Processes, School of Chemistry and Molecular Engineering, East China Normal University, Shanghai 200062, China*

[b] *Institute of Eco-Chongming, Shanghai 202162, China*

[c] *School of Energy and Materials, Shanghai Polytechnic University, Shanghai, 201209, China*

Corresponding author: Prof. Yueming Liu

Tel/Fax: +86-21-6223-2058;

E-mail: ymliu@chem.ecnu.edu.cn (Y.M. Liu)

Table S1. The superior solvents on various oxidations reactions catalyzed by titanosilicates with H_2O_2 as the oxidant.

Catalyst	Linear alkenes	Cyclopentene	Cyclohexene	Allyl alcohol	Cyclohexanol	Diallyl ether	1,4-dioxane	2,5-DHF	pyridine	NH_3	Phenol	Aliphatic hydrocarbon	Sulfides	B-V oxidation
TS-1	MeOH	MeOH	MeCN	MeOH/ H_2O		MeCN/ Acetone	Non-solvent	MeCN/ H_2O	MeOH/ H_2O/ Non-solvent	*t*-BuOH	Acetone	*t*-BuOH		Non-solvent
Ti-MWW	MeCN	MeCN/ MeOH	MeCN/ MeOH	MeCN/ H_2O		MeOH/ Acetone	Non-solvent	MeOH	Non-solvent	*t*-BuOH			Non-solvent	
Ti-Beta	MeCN	MeOH/ EtOH	MeOH	MeOH/ EtOH	MeCN					*t*-BuOH			MeCN	
Reference	1-4	5, 6	1	7	8	6	9	10, 11	12	13-15	16, 17	18	19, 20	21, 22

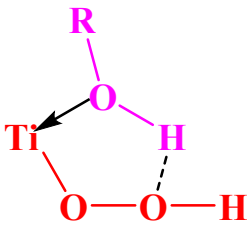

Species I

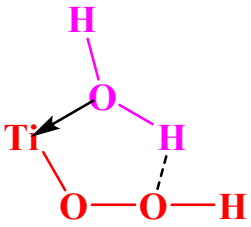

Species II

Five-membered ring structures

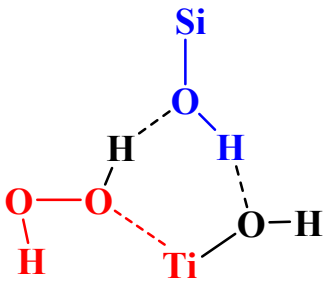

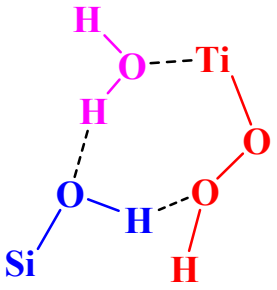

Six-membered ring structures **Seven-membered ring structures**

Scheme S1. Solvent promotes the stability of Ti-OOH intermediate through the formation of the five-membered ring (5MR, Species Ⅰ [23] and Species Ⅱ [8]), six-membered ring (6MR) [24], or seven-membered ring (7MR) structures [25].

Section S1. Catalysts characterizations.

All samples were obtained after calcining and then were measured as soon as possible through various characterization methods. The X-ray diffraction (XRD) patterns were measured under ambient conditions on a Rigaku Ultima IV diffractometer using Cu Kα radiation (1.5406 Å) and a nickel filter in the 2 θ angle range from 5° to 35° at 35 kV and 25 mA. The UV-Visible diffuse reflectance spectra (UV/Vis) were recorded under ambient conditions on a Shimadzu UV-2400PC spectrophotometer using $BaSO_4$ plate as a reference. Inductively coupled plasma optical emission spectroscopy (ICP-OES) was performed on a Thermo IRIS Intrepid II XSP atomic emission spectrometer. Scanning electron microscopy (SEM) was performed by a Hitachi S-4800 microscope. Nitrogen adsorption was taken with a BEL-MAX instrument at 77 K, and all samples were treated at 573 K for 6 h in vacuum before adsorption−desorption. The ^{29}Si solid-state MAS NMR spectra were recorded on a VARIAN VNMRS-400WB spectrometer under a one-pulse condition. The spectra were obtained with a frequency of 79.43 MHz, a spinning rate of 3000 rps, and a recycling delay of 60 s. ^{19}F MAS NMR spectra were acquired at 9.4 T on a Varian Infinity Plus 400 WB spectrometer using a 2.5 mm HX MAS probe. The chemical shifts were referenced to trifluoroacetic acid at -76.55 ppm. The ^{1}H MAS NMR spectra were obtained after the treatment at 723 K for 2 h in vacuum with a frequency of 400.1 MHz, a spinning rate of 10000 rps, and the chemical shift was referred to TMS($(CH_3)_4Si$). The infrared spectra (IR) were obtained on a Nicolet NEXUS 670 spectrometer with 2 cm^{-1} resolution. The spectra in the framework vibration region of titanosilicates were recorded with KBr technique at 298 K. The spectra in the hydroxyl stretching region were collected at ambient temperature after the treatment at 723 K for 2 h in vacuum. For the pyridine spectra measurement (1000-4000 cm^{-1}), it was recorded as follows: a self-supported wafer (9.6 $mg \cdot cm^{-1}$ thickness and 2 cm in diameter) was set in a quartz IR cell sealed with CaF_2 windows connected with a vacuum system. After the sample was evacuated at 723 K for at least 2 h, the pyridine adsorption was carried out by exposing the wafer to pyridine vapor

(1.3 kPa) at 298 K for 20 min. The physisorbed and chemisorbed pyridine was then removed by evacuation at different temperatures (373 K–523 K) for 0.5 h, and the corresponding spectra were collected at room temperature. Thermogravimetric analysis (TGA) was carried out with TGA/SDTA851e thermogravimetric analyzer produced by Mettler-Toledo Company in air atmosphere. The test range was from 35 °C to 800 °C, and the heating rate was 10 °C/min. The UV Raman spectra were recorded on UV-RAMAN100 Raman spectrometer made by Beijing ZOLIX INSTRUMENTS CO. LTD. A 244-nm line of a LEXEL laser of a He-Gd laser was used as the excitation source.

Section S2.

S2.1. Elimination of the limitations of internal and external diffusion from the fixed-bed reactor.

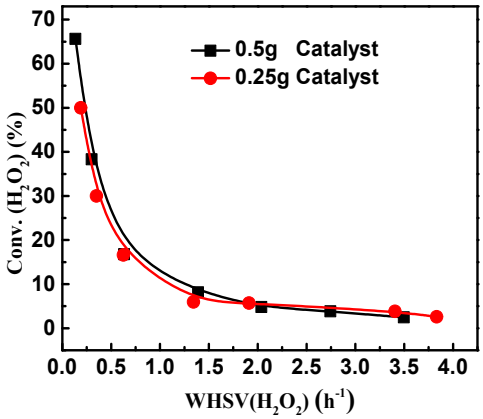

Fig. S1. External diffusion test of the catalyst. Reaction conditions: TS-1 (40–80 mesh), 0.5 g; *w*(H_2O_2), 2 %; WHSV(H_2O_2), 0.1–4.0 h^{-1}; solvent, MeOH; 333 K.

To eliminate the limitation of external diffusion from the fixed-bed reactor, we investigated the influence of the space velocity of H_2O_2 on H_2O_2 activation. Figure S1 shows that when the space velocity of H_2O_2 varied from 0.1 h^{-1} to 4.0 h^{-1}, the relation curves that H_2O_2 conversion with the space velocity of H_2O_2 almost coincided. It implies that the limitation of external diffusion is eliminated, and the space velocity of H_2O_2 was selected as 0.3 h^{-1} in the subsequent experiments.

Table S2. Internal diffusion test of the catalyst.

Entry	The mesh of catalysts	H_2O_2 Conversion (%)
1	16–20	32.1
2	20–26	34.7
3	26–40	37.9
4	40–80	38.3

Reaction conditions: TS-1, 0.5 g; *w*(H_2O_2), 2 %; solvent, MeOH; WHSV(H_2O_2), 0.3 h^{-1}, 333 K, TOS (time on stream), 10 min.

To eliminate the limitation of internal diffusion from the fixed-bed reactor, we investigated the influence of the mesh of catalysts on H_2O_2 activation. Table S2 shows that increasing the mesh of catalysts improves H_2O_2 conversions and when the mesh varied from 26 to 80, H_2O_2 conversion is almost unchanged, indicating that the limitation of internal diffusion is eliminated. In our subsequent experiments, the mesh of catalysts was selected as 40–80.

S2.2. Determination of reaction order, reaction rate (r), reaction rate constants (k), the activation energies (E_a), and pre-exponential factors (A) on H_2O_2 activation reaction.

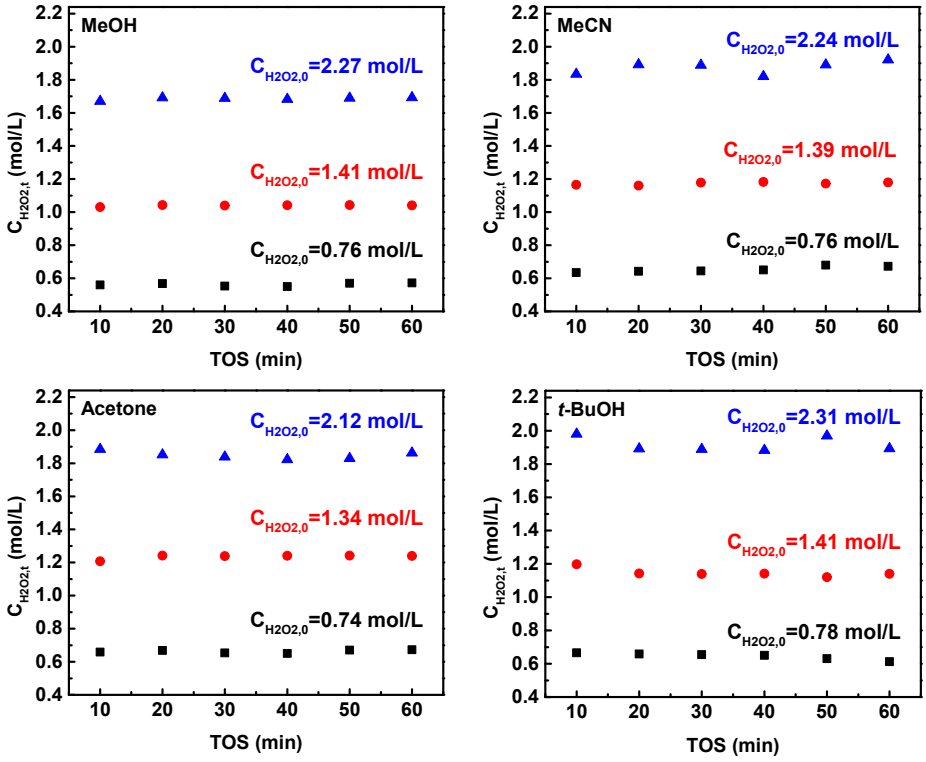

Fig. S2. Effect of time on stream (TOS) on the concentration of H_2O_2 on H_2O_2 activation in various initial H_2O_2 concentrations in different solvents (MeOH, MeCN, Acetone, and *t*-BuOH) in a fixed-bed reactor (10mL). Reaction conditions: TS-1 3 g, H_2O_2 space velocity 0.3 h^{-1}, 318 K.

Table S3. Activation reaction of H_2O_2 over TS-1 in different solvents.

Entry	Solvent	$C_{H2O2,0}$ (mol/L)	$C_{H2O2,t}$ (mol/L)	ΔC_{H2O2} (mol/L)	$r_{H2O2\ activation}$ (*10^{-5} mol·L^{-1}·s^{-1})
1		0.76	0.56	0.20	18.86
2	MeOH	1.41	1.03	0.38	19.12
3		2.27	1.67	0.60	18.94
4		0.76	0.63	0.12	11.63
5	MeCN	1.39	1.17	0.23	11.58
6		2.24	1.87	0.37	11.69
7		0.74	0.66	0.08	7.52
8	Acetone	1.34	1.21	0.13	6.96
9		2.12	1.88	0.23	7.85
10		0.78	0.67	0.11	10.07
11	*t*-BuOH	1.41	1.20	0.21	10.57
12		2.31	1.98	0.33	10.14

Reaction conditions: TS-1 3 g, H_2O_2 space velocity 0.3 h^{-1}, 318 K

The activation rate of H_2O_2 (r) can be calculated by the following equation.

$$r = kC_{H_2O_2}^{\alpha} C_{cat}^{\beta}$$

k is the reaction rate constant, C_{H2O2} and C_{cat} are the concentration of H_2O_2 and catalyst, respectively, α and β are the H_2O_2 activation reaction order with respect to H_2O_2 and catalyst, respectively.

The activation rate of H_2O_2 (r) can also be calculated as follows:

$$-r = \frac{d(C_{H2O2})}{d(V/F_v)}$$

F_v is the flow rate of volume (L/s) and V is the reactor volume (L).

We tested the reaction rates on the H_2O_2 activation reaction in different H_2O_2 concentrations in different solvents (MeOH, MeCN, Acetone, and *t*-BuOH) in a fixed bed. Figure S2 shows the effect of time on stream (TOS) on the concentration of H_2O_2 on H_2O_2 activation in various initial H_2O_2 concentrations in different solvents in a fixed-bed reactor. The results show that the concentration of H_2O_2 is almost constant

with varying TOS when the solvent and initial H_2O_2 concentration are certain. It means that the deactivation of the H_2O_2 activation reaction is not obvious and the subsequent apparent reaction rate of the H_2O_2 activation was determined from the initial reaction rate (TOS = 10 min). As shown in Table S3, when the solvent is MeOH, with increasing the concentration of H_2O_2, the concentration difference of H_2O_2 ($\Delta C_{H2O2} = C_{H2O2,0} - C_{H2O2,t}$) before and after the H_2O_2 activation reaction increases, however, the reaction rate of the H_2O_2 activation is almost identical (~$19*10^{-5}$ $mol \cdot L^{-1} \cdot s^{-1}$) as the H_2O_2 concentrations change. It implies that the H_2O_2 activation reaction order with respect to H_2O_2 is zero. The same results are observed when the solvents are MeCN, Acetone, or *t*-BuOH, and the reaction rate of H_2O_2 activation increases in the order of Acetone < *t*-BuOH < MeCN < MeOH (Table S3), in line with the order of 1-hexene epoxidation activity over TS-1 (Table 1). Based on these results, the apparent reaction rate constants of the H_2O_2 activation were determined from the initial reaction rate, and the activation energies (E_a) and pre-exponential factors (A) were thus determined from a linear fitting method of the reaction rate constants in different reaction temperatures, according to the Arrhenius equation.

Section S3. Investigation of the influence of solvent on heterogeneous catalysis of 1-hexene epoxidation.

Solvent strongly influences the catalytic performance in titanosilicates/H_2O_2 oxidation system, however, its role remains unclear to date. We investigated the influence of solvent on diffusion, adsorption/desorption, and surface reaction, based on the heterogeneous catalysis process via a typical probe reaction with the epoxidation of 1-hexene.

S3.1. The influence of solvent on diffusion.

In microporous zeolites, solvent molecules might affect the diffusion of reactants in the catalyst, especially for liquid-phase conditions where the zeolite pores are essentially full of molecules. In general, the external diffusion limitation can be avoided under vigorous stirring conditions. To investigate the intraparticle mass transfer limitations, we prepared a series of TS-1-x (x represents the molar ratio of TPAOH/SiO_2) catalysts with different crystallite sizes by varying the ratio of TPAOH/SiO_2 from 0.08 to 0.18 by hydrothermal synthesis method [26] and tested the 1-hexene epoxidation in four typical solvents (MeOH, MeCN, acetone, and *t*-BuOH). All TS-1 samples are crystallized well (Fig. S3A) and framework Ti coordination (Fig. S3B and S3C), while the particle size and pore structure are varied (Fig. S4 and Table S4). Figure S4 shows that as the ratio of TPAOH/SiO_2 increases, the particle size of TS-1-x decreases from ~3.5 μm to ~0.2 μm. Table S4 shows that as the ratio of TPAOH/SiO_2 increases, TS-1-x has the similar micropore volumes of 0.154~0.162 $cm^3 \cdot g^{-1}$ and micropore surface area of 348~362 $m^2 \cdot g^{-1}$. However, their external surface area increases from 26 $cm^3 \cdot g^{-1}$ to 77 $cm^3 \cdot g^{-1}$ (Table S4), due to the deceased particle size (Figure S4). TS-1-x shows different activity in alkenes epoxidation and conversion of 1-hexene increases from 14.2% to ~25% in MeOH solvent with particle size decreasing and external surface area increasing (Table S4). When the particle size of TS-1 is less than 1.2 μm, its oxidation activity reaches a high level and does not change distinctly (Table S4, entries 1–3). And when the used solvents are

MeCN, acetone, and *t*-BuOH, the same results are observed as that in MeOH solvent. It is supported by the previous report [27] that the epoxidation of small alkenes (e.g., 1-hexene) was diffusion unlimited when the crystal size of zeolite was small, based on analysis of the Weisz modulus. These results indicate that the intraparticle mass transfer limitations have little effect on 1-hexene epoxidation when the particle size of TS-1 is less than 1.2 μm, however, it presents distinctly different activity in different solvents. Therefore, the diffusion is not mainly responsible for the different catalytic performances of TS-1 with the 10-membered ring (10MR) pore structure for 1-hexene epoxidation in different solvents. As for other titanosilicates including Ti-MWW (10MR and 12MR) and Ti-Beta (12MR), the diffusion can be thus ignored. To assure unlimited diffusion, the ratio of TPAOH/SiO_2 is 0.15 and the crystal size of the applied titanosilicates is about 0.5–0.6 μm in the subsequent study.

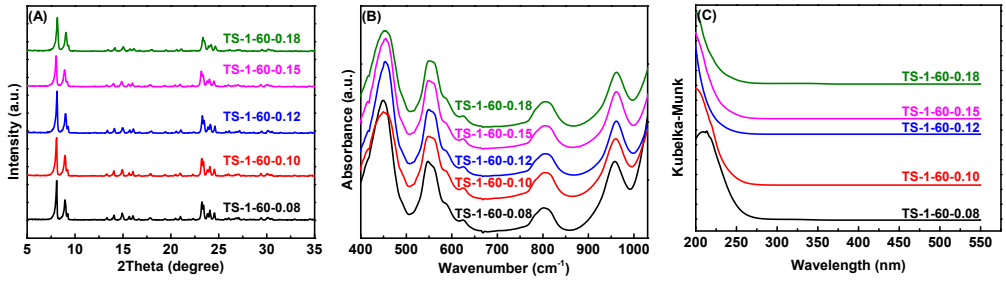

Fig. S3. XRD (A), IR (B), and UV-Vis (C) spectra of TS-1 under the different ratios of TPAOH/SiO_2.

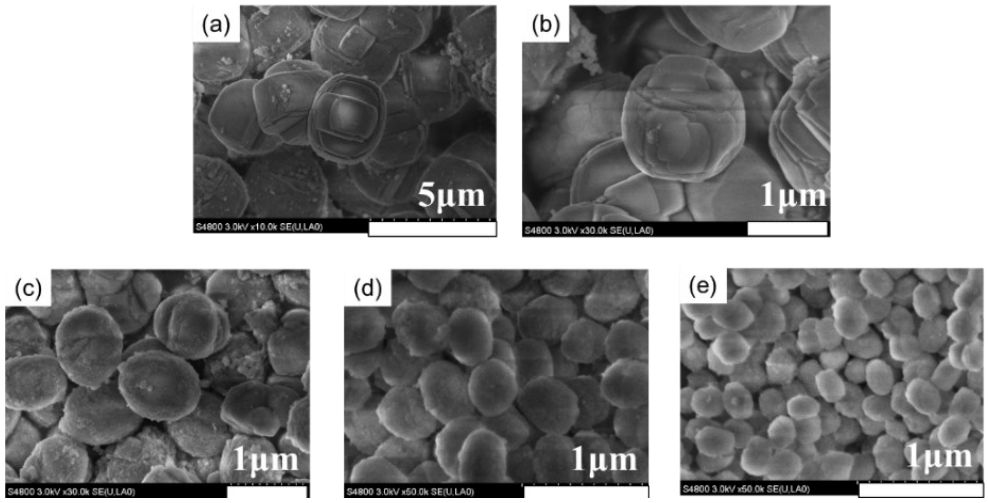

Fig. S4. SEM images of TS-1-60-x (60 represents the Si/Ti ratio and x represents the molar ratio of TPAOH/SiO_2) under different crystallite sizes. (a) TS-1-60-0.08, (b) TS-1-60-0.10, (c) TS-1-60-0.12, (d) TS-1-60-0.15, (e) TS-1-60-0.18.

Table S4. The catalytic performance of 1-hexene epoxidation over a series of TS-1-60-x (60 represents the Si/Ti ratio and x represents the molar ratio of TPAOH/SiO_2) catalysts with different crystallite sizes in various solvents.

Entry	Catalyst	Si/Ti [a]	Particle size(μm)[b]	V_{micro}[c]	S_{micro}[c]	S_{exter}[c]	MeOH[d]	MeCN[d]	Acetone[d]	*t*-BuOH[d]
1	TS-1-60-0.18	62	0.2-0.3	0.160	361	77	24.9 (185)	16.7 (124)	7.1 (53)	14.2 (106)
2	TS-1-60-0.15	62	0.5-0.6	0.162	362	67	25.5 (190)	17.3 (129)	7.7 (57)	15.5 (115)
3	TS-1-60-0.12	61	~1.2	0.154	348	58	25.3 (185)	16.1 (118)	7.5 (55)	15.0 (110)
4	TS-1-60-0.10	60	~2.0	0.154	350	36	20.1 (145)	14.9 (107)	5.5 (40)	14.7 (106)
5	TS-1-60-0.08	55	~3.5	0.154	352	26	14.2 (94)	12.6 (83)	3.8 (25)	12.7 (84)

[a] Determined by ICP. [b] Given by SEM. [c] Calculated by BET method and *t*-plot method. V_{micro} ($cm^3 \cdot g^{-1}$), S_{micro} ($m^2 \cdot g^{-1}$), and S_{exter} ($m^2 \cdot g^{-1}$) stand for microporous volume, microporous surface area, and external surface area, respectively. [d] epoxidation conditions: catalyst 50 mg, solvent 10 mL, H_2O_2 (30 wt % aqueous solution) 10 mmol, 1-hexene 10 mmol, 333 K, 2 h. The 1-hexene conversions were outside of parentheses and the turnover numbers (TONs) per Ti site for 1-hexene conversion were enclosed in parentheses.

S3.2. The influence of solvent on adsorption/desorption.

The adsorption of reactants and desorption of products are essential steps in heterogeneous catalysis. Through a tracer chromatographic method, Langhendries et al. [28] measured that the adsorption of 1-hexene over TS-1 in different solvents decreased in the order of MeOH > EtOH > MeCN > acetone > 1-PrOH, and the corresponding performance of 1-hexene epoxidation decreased in the order of MeOH >> MeCN, acetone > EtOH > 1-PrOH. Ramachandran [29] and Jiao [30] supported that solvent could affect the adsorption of the reactants and hence the reaction rate. Here, we tested the 1-hexene epoxidation, 1-hexene adsorption, and H_2O_2 adsorption [31] over TS-1 and compared their order in different solvents. The 1-hexene epoxidation rate over TS-1 followed the order: MeOH > MeCN > EtOH > *t*-BuOH > Acetone (Fig. S5A). Figure S5B shows that TS-1 presents different adsorption ability of 1-hexene in different solvent (MeOH > EtOH> MeCN > Acetone > *t*-BuOH). It suggests that

solvent can affect the adsorption ability of 1-hexene, in line with the previous report [28]. However, this adsorption order is not relevant to the order of 1-hexene epoxidation rate. Fig. S5C shows H_2O_2 adsorption ability over TS-1 in various solvents. Similar results were also observed that the H_2O_2 adsorption order is also not relevant to the order of 1-hexene epoxidation rate. So the adsorptions of 1-hexene and H_2O_2 are not mainly responsible for the phenomenon of solvent effect over titanosilicates/H_2O_2 system.

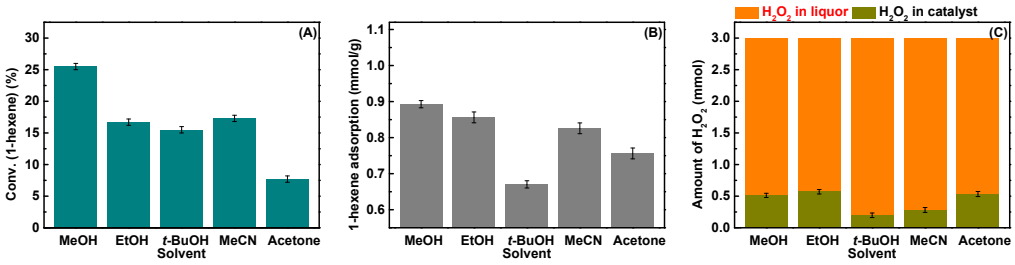

Fig. S5. The 1-hexene epoxidation (A), 1-hexene adsorption (B), and the liquid-phase H_2O_2 adsorption (C) over TS-1 in protic and aprotic solvents. 1-hexene epoxidation conditions: catalyst 50 mg, solvent 10 mL, H_2O_2 (30 wt % aqueous solution) 10 mmol, 1-hexene 10 mmol, 333 K, 2 h. The 1-hexene adsorption with catalyst (0.1 g) and 1 wt.% 1-hexene in solvent (3 g) was held under vigorous stirring conditions at 313 K for 1 h. The residual 1-hexene was measured by GC. H_2O_2 adsorption was carried out in the ice-water bath and the dark condition to avoid H_2O_2 decomposition. The H_2O_2 adsorption with catalyst (0.05 g), solvent (5 mL), and H_2O_2 (30 wt % aqueous solution, 3 mmol) was held under vigorous stirring conditions at 273 K for 1 h. The residual free H_2O_2 was titrated by $Ce(SO_4)_2$ solution.

In general, the hydrophobic surface of titanosilicates could help adsorb and enrich organic reactants to bring about a high catalytic activity [32-34]. We prepared the hydrophobic R-Ti-MWW-cal by reversible structural rearrangement to investigate the influence of hydrophobicity of titanosilicates on 1-hexene epoxidation [34]. Table S5 shows that R-Ti-MWW-cal presents a higher 1-hexene epoxidation activity as Ti-MWW in MeCN and acetone, though it hasn't changed much with MeOH and *t*-BuOH as the solvent. It's worth noting that both Ti-MWW and R-Ti-MWW-cal have

excellent epoxidation performance in aprotic MeCN and acetone. These results indicate that the hydrophobicity of titanosilicates can affect the epoxidation activity, however, it is not mainly responsible for solvent effect over titanosilicates/H_2O_2 system.

Table S5. The catalytic performance of 1-hexene epoxidation over Ti-MWW and R-Ti-MWW-cal catalysts in various solvents.

Entry	Catalyst	Si/Ti[a]	Si/B[a]	MeOH[b]	MeCN[b]	Acetone[b]	*t*-BuOH[b]
1	Ti-MWW	52	46	12.3 (77)	42.6 (266)	38.2 (238)	19.9 (124)
2	R-Ti-MWW-cal	52	49	11.1 (69)	52.5 (328)	44.3 (276)	20.4 (126)

[a] Determined by ICP. [b] Epoxidation conditions: catalyst 50 mg, solvent 10 mL, H_2O_2 (30 wt % aqueous solution) 10 mmol, 1-hexene 10 mmol, 333 K, 2 h. The 1-hexene conversions were outside of parentheses and the turnover numbers (TONs) per Ti site for 1-hexene conversion were enclosed in parentheses.

The desorption of epoxides has an important effect on the whole catalytic cycle. Zhou et al. [35] proposed that the desorption of the epoxide product and the recovery of the Ti-OH species were the rate-determining steps in the overall reaction. Ti-η^2(OOH)-MeCN had lower desorption energy than Ti-η^2(OOH)-H_2O, suggesting that the MeCN solvent was favorable for 1-hexene epoxidation in Ti-MWW. However, this result has not been confirmed experimentally. To explore the influence of solvent on the desorption of epoxide, we treated TS-1 with 1,2-epoxyhexane in toluene to obtain the epoxide-adsorption sample (TS-1-epo) and desorb it with the washing of different solvents to obtain epoxide-desorption samples (epo-solvent). Thermogravimetric (TG) analysis was carried out to test the adsorbing content of 1,2-epoxyhexane. The weight loss below 100 °C was attributed to the desorption of water, while the weight loss from 200 to 400 °C was assigned to the desorption of 1,2-epoxyhexane. Compared to the pristine TS-1, TS-1-epo presents a distinct weight loss from 200 to 400 °C (12.3% in Fig. S6), indicating that 1,2-epoxyhexane can adsorb strongly on the surface and channels of TS-1. By subsequent washing with various

solvents, this weight loss decreased obviously (Fig. S6). It implies that the introduction of organic solvents promotes the desorption of the product epoxides (e.g. 1,2-epoxyhexane) and the promotion over different solvents is different. Especially, when the used solvent is *t*-BuOH, the weight loss decreases to 6.1%, indicating its strong ability in desorbing 1,2-epoxyhexane (Fig. S6). However, the rate of 1-hexene epoxidation in different solvents is not relevant to the promotion of 1,2-epoxyhexane desorption so the effect of solvent on the desorption of the product epoxides is not mainly responsible for the phenomenon of solvent effect over titanosilicates/H_2O_2 system.

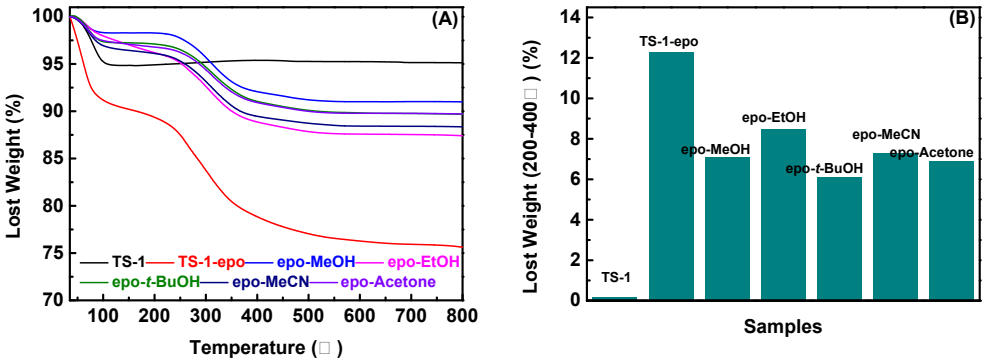

Fig. S6. TG curves (A) and the lost weight from 200 to 400 °C (B) of TS-1, TS-1-epo, and epo-solvent samples. TS-1-epo was obtained by the post-treatment of TS-1 into a solution that contained 1,2-epoxyhexane with the following composition: 0.3 g TS-1, 10 mL toluene, and 0.3 g 1,2-epoxyhexane. The mixture was stirred at 333 K for 1 h. Then the resulting solid was recovered by filtration, drying at 353 K for 8 h to obtain TS-1-epo. Then the obtained TS-1-epo was washed with different solvents (MeOH, EtOH, *t*-BuOH, MeCN, and acetone) with the following composition: 0.08 g TS-1 and 10 mL solvent. The mixture was stirred at 333 K for 1 h. Then the resulting solid was recovered by filtration, drying at 353 K for 8 h to obtain epo-solvent.

S3.3. The influence of solvent on surface reaction.

Generally, the surface reaction of 1-hexene epoxidation included the H_2O_2 activation to form the Ti-OOH intermediate and the further transfer of active "O" to the reactant 1-hexene [23, 25, 36, 37]. Solvents have been found to directly participate in the

oxidation process through the complex interactions among substrates, solvents, and the structure of Ti active sites in titanosilicates [1, 23, 38-41].

S3.3.1. The influence of solvent on the stability of Ti-OOH and the transfer of active "O" to the reactant.

Clerici et al. proposed that MeOH helped to form a stable 5MR structure (species Ⅰ) by the coordination of MeOH to Ti centers and hydrogen bonding to Ti-peroxo complex for the hydrophobic TS-1, thereby improving the epoxidation activity [23]. Whereas the catalytic activity of relatively hydrophilic Ti-Beta and Ti-MWW is improved in MeCN solvent due to the stable species Ⅱ formed by the coordination and hydrogen bonding of H_2O to Ti-OOH intermediate [1, 8]. Vayssilov and van Santen compared different 5MR adsorption species from the interaction of Ti-OOH intermediate and MeOH, water (H_2O), or a silanol (Si-OH) group. They revealed that MeOH promoted the formation of the 5MR structure than H_2O and Si-OH species [24]. However, the formations of these 5MR structures were difficult with the high energy barrier of 90−130 kJ/mol [24] and there is no solid evidence to prove the existence of these intermediate to date. Using DFT calculation method based on cluster models of Ti-MWW, Zhou et al. suggested that the six-coordinated Ti-η^2(OOH)-MeCN intermediate was more stable than the five-coordinated Ti-η^2(OOH) intermediate [35]. Although these views can rationalize the partial phenomenon of solvent effect, the interpretation of catalytic results when using a bigger group of solvents of different natures was in general not satisfactory or incomplete.

The transfer ability of active "O" to the reactant alkenes is related to the nucleophilicity of alkenes, the electrophilicity of the catalysts, and the polarity of solvents [42]. Strong nucleophilicity of alkenes and strong electrophilicity of the catalyst favors the transfer of electrophilic oxygen to nucleophiles. When the reactant alkene and catalyst are fixed, with the increase of solvent polarity, the heterolytic cleavage of O-O bond in Ti-OOH intermediate for the transfer of active "O" was promoted, based on the Hughes-Ingold rules [43]. Based on our previous work [42], once the Ti-OOH

species were formed, the two reaction pathways between the subsequent transfer of active "O" to reactant (pathway Ⅱ) and the oxidative decomposition of H_2O_2 with Ti-OOH species (pathway Ⅰ) were competitive (Scheme S2). This competition determined the utilization efficiency of H_2O_2. Table S6 shows that the differences in utilization efficiency of H_2O_2 on 1-hexene epoxidation in various solvents over TS-1 and Ti-MWW zeolites are not large, though the epoxidation activities vary obviously. It suggests that the effect of solvent on the transfer pathway can not explain the phenomenon of solvent effect. Besides, both the order of the epoxidation activities for TS-1 (MeOH > MeCN > *t*-BuOH > Acetone in Table S6, entries 1–4) and the order for Ti-MWW (MeCN > Acetone > *t*-BuOH > MeOH in Table S6, entries 5–8) are inconsistent with the order of solvent polarity (MeCN > MeOH > Acetone > *t*-BuOH), supporting the above viewpoint.

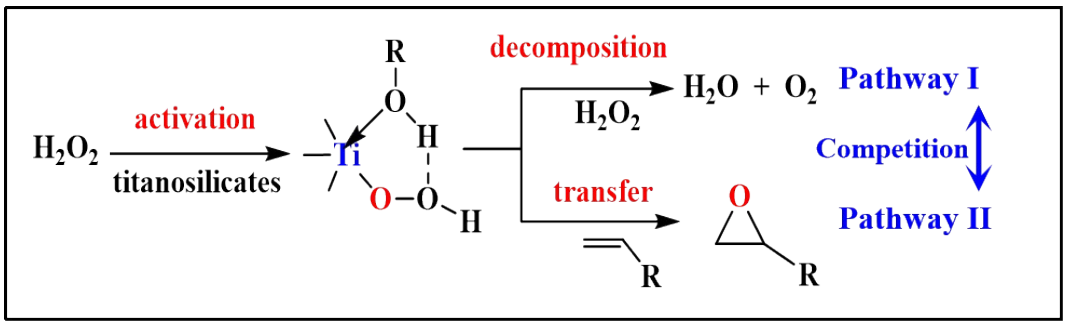

Scheme S2. The reaction pathways of H_2O_2 during the alkenes epoxidation catalyzed by titanosilicates [42].

Table S6. The epoxidation of 1-hexene over TS-1 and Ti-MWW in various solvents.

Entry	Catalyst	Solvent	1-Hex Conv. (%)	H_2O_2 Conv. (%)	Oxide Sel. (%)	H_2O_2 Eff. (%)
1	TS-1	MeOH	25.5	30.0	92.3	85.0
2		MeCN	17.3	21.0	100	82.5
3		Acetone	7.7	10.9	100	70.6
4		*t*-BuOH	15.5	18.6	100	83.3
5	Ti-MWW	MeOH	12.3	15.6	87.2	78.9
6		MeCN	42.6	48.0	100	88.8
7		Acetone	38.2	49.6	100	77.0

8	*t*-BuOH	19.9	24.2	100	82.1

The epoxidation reaction conditions: catalyst, 50 mg; solvent, 10 mL; 1-hexene, 10 mmol; H_2O_2 (30 wt % aqueous solution), 10 mmol; 333 K; 2 h.

S3.3.2. The influence of solvent on H_2O_2 activation to form Ti-OOH

Based on DFT theoretical results, the apparent activation energy of H_2O_2 activation to form Ti-OOH is high, which implied that the H_2O_2 activation process was regarded as the rate-determining step of the global epoxidation reaction [24, 25, 39, 44, 45]. Employing the in situ UV Raman spectroscopic study for propylene epoxidation on TS-1, Guo et al. observed an excellent consistency between the area of characteristic peak at 837 cm^{-1} assigned to O−O stretching mode in the Ti-η^2(OOH) active intermediate and the formation rate of product PO [46]. Besides, solvent only affected the intensity of characteristic peak at 837 cm^{-1} but not the peak site (e.g., the solvent MeOH generated the Ti-OOH species faster than H_2O) [46]. These results indicated that the selection of solvent altered the formation of the Ti-OOH species for H_2O_2 activation without changing the identity of Ti-OOH species, thereby affecting the epoxidation activity. Besides, the activities on H_2O_2 activation and 1-hexene epoxidation over TS-1 in different solvents increase in the almost similar order of acetone < *t*-BuOH < MeCN < MeOH (Table 1), which implies that solvent plays a role in the catalytic oxidation process by affecting the H_2O_2 activation. Therefore, we studied solvent effect by mainly focusing on the role of solvents on H_2O_2 activation in this work.

Section S4. Characterization of TS-1, TS-1^s, Ti-MWW, and F-Ti-MWW.

Figure S7A presents XRD spectra of TS-1, TS-1^s, Ti-MWW, and F-Ti-MWW zeolites. The results show that TS-1 and TS-1^s samples have the typical MFI topological structure, while Ti-MWW and F-Ti-MWW samples have the three-dimensional MWW structure, and all samples contain no impurity of other zeolite phases. Figure S8 shows that the surface of TS-1^s becomes rougher, compared with the smooth surface of TS-1, consistent with our previous work [47]. Both Ti-MWW and F-Ti-MWW samples keep a typical platelet-shaped morphology (Fig. S8). Table S7 presents the pore structure property and element composition measured by N_2 adsorption-desorption techniques and ICP data. It can be seen that all samples have a good pore structure, and the Si/Ti ratios of TS-1 and TS-1^s are around 75, while Ti-MWW and F-Ti-MWW samples have the almost same Si/Ti ratio of around 52 (Table S7, entries 1, 5–7). For the pore size distribution, all samples contain no impurity of other zeolite phases from the XRD data in Figure S7A so the pore size distribution depends on the channel size of zeolites themselves. Pore sizes of TS-1 and TS-1^s are 0.51× 0.55 nm for the sinusoidal channel and 0.53× 0.56 nm for the straight channel [48], while those of Ti-MWW and F-Ti-MWW are 0.41 nm× 0.51 nm for the sinusoidal channel and 0.71 nm× 0.71 nm× 1.81 nm for 12-MR supercages [49].

Figure S7B shows the UV-Vis spectra of TS-1, TS-1^s, Ti-MWW, and F-Ti-MWW zeolites, and the corresponding deconvolution bands and results are shown in Fig. S9 and Table S8. The bands at 203 nm, 230 nm, and 270 nm were attributed to the "closed" tetrahedrally coordinated titanium species ($Ti(OSi)_4$), the "open" tetrahedral titanium ($Ti(OSi)_3OH$) species, and octahedral "TiO_6" species, respectively [50]. Figure S9 shows that the Ti active site of TS-1 is mainly $Ti(OSi)_4$ species at 203 nm. Besides $Ti(OSi)_4$ species, TS-1^s possesses the "open" tetrahedral titanium ($Ti(OSi)_3OH$) species at 230 nm from the transformation of $Ti(OSi)_4$ species via the selective dissolution and simultaneous recrystallization of dissolved Si species [47]. As for Ti-MWW and F-Ti-MWW zeolites, the band at 230 nm indicates that they

possess abundant "open" $Ti(OSi)_3OH$ species (Fig. S9). The ^{19}F MAS NMR spectrum of F-Ti-MWW contains the band at 152.8 ppm (Fig. S7C) attributed to $SiO_{3/2}F$ species [51, 52], indicating that F species is introduced to the zeolite framework.

Therefore, there is no evident difference in basic physicochemical properties among TS-1 and TS-1^s zeolites. The Ti active site of TS-1 is mainly $Ti(OSi)_4$ species, while TS-1^s also contains $Ti(OSi)_3OH$ species besides $Ti(OSi)_4$ species. F-Ti-MWW presents a similar physicochemical property to Ti-MWW, and both of them possess abundant "open" $Ti(OSi)_3OH$ active species. Owing to the electronic withdrawing ability of F atoms, the introduced F species improves the electropositivity of the Ti sites [51, 52], implying that F-Ti-MWW possesses a stronger Lewis acidity than Ti-MWW.

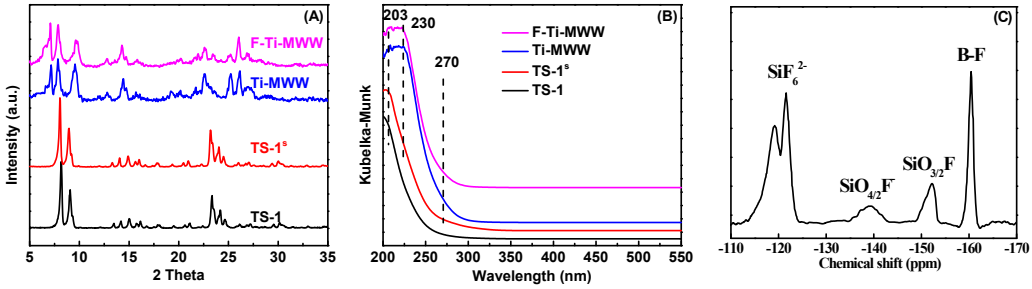

Fig. S7. XRD (A) and UV-Vis (B) spectra of TS-1, TS-1^s, Ti-MWW, and F-Ti-MWW zeolites; ^{19}F MAS NMR spectrum of F-Ti-MWW zeolite (C).

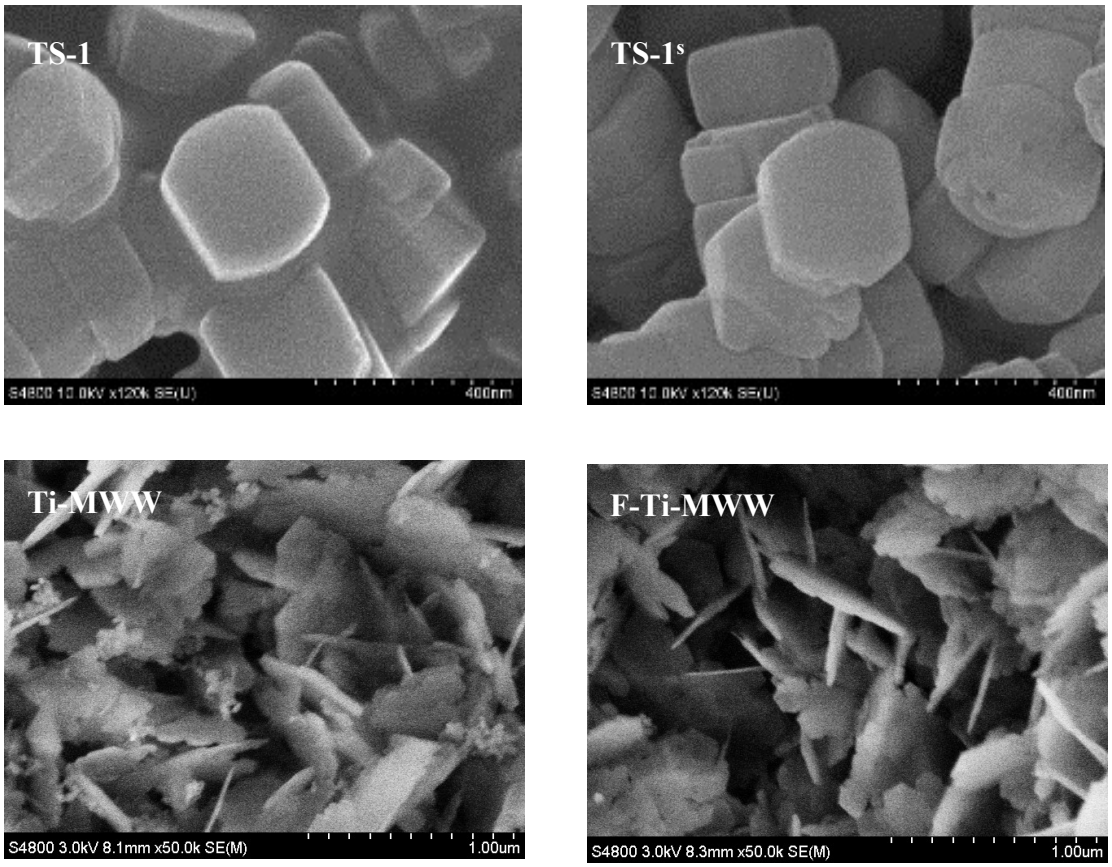

Fig. S8. SEM images of TS-1, TS-1^{s}, Ti-MWW, and F-Ti-MWW zeolites.

Table S7. Physicochemical properties of TS-1, TS-1^{s}, Ti-MWW, and F-Ti-MWW zeolites.

Entry	Catalyst	S_{micro}[a]	V_{micro}[a]	V_{meso}[a]	Si/Ti[b]
1	TS-1 (TS-1A)	407	0.179	0.102	75
2	TS-1^{s} (TS-1E)	350	0.154	0.082	75
3	Ti-MWW	390	0.174	0.700	52
4	F-Ti-MWW	383	0.179	0.710	51

[a] Calculated by BET method and t-plot method. S_{micro} ($m^2 \cdot g^{-1}$), V_{micro} ($cm^3 \cdot g^{-1}$), and V_{meso} ($cm^3 \cdot g^{-1}$) stand for microporous surface area, microporous volume, and mesoporous volume, respectively.
[b] Detected by ICP.

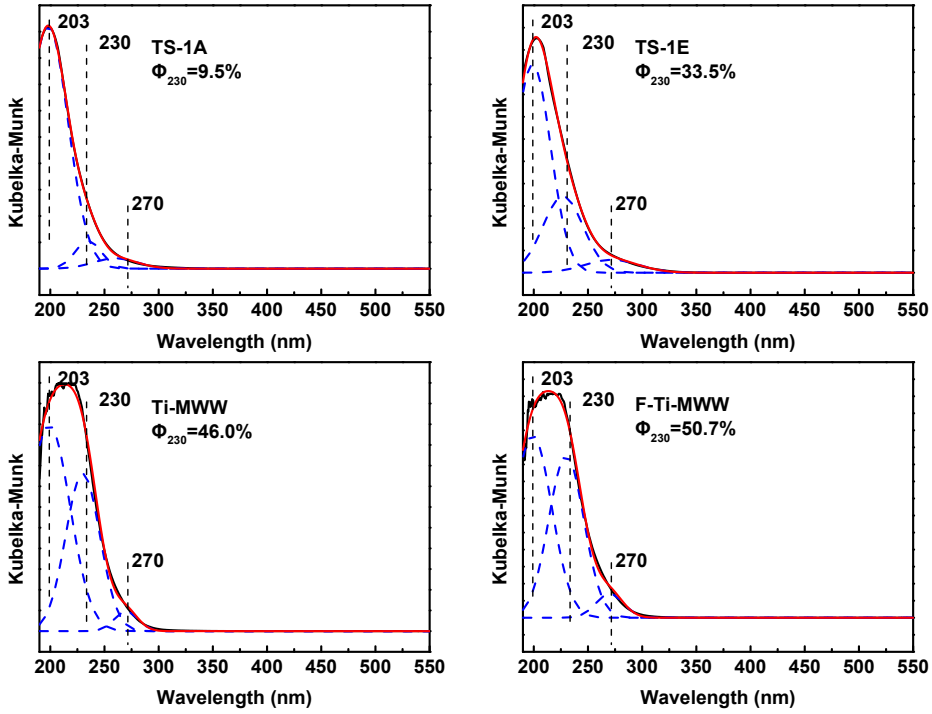

Fig. S9. The deconvolution band at 203 nm, 230 nm, and 270 nm in UV-Vis spectra of TS-1, TS-1^{s}, Ti-MWW, and F-Ti-MWW samples. Φ_{230} is the ratio of the peak area at 230 nm to the total area. $\Phi_{230} = A_{230}/(A_{203+}A_{230+}A_{270})$. The detailed UV-Vis peak deconvolution were shown in Table S8.

Table S8. Details of the UV-Vis peak deconvolution of various zeolites from Fig. S9.

Entry	Catalyst	Φ_{203}(FWHM$_{203}$)	Φ_{230}(FWHM$_{230}$)	Φ_{270}(FWHM$_{270}$)
1	TS-1A	84.6 (43)	9.5 (30)	5.9 (47)
2	TS-1E	58.8 (40)	33.5 (34)	7.7 (51)
3	Ti-MWW	50.0 (45)	46.0 (37)	4.0 (28)
4	F-Ti-MWW	43.4 (43)	50.7 (38)	5.9 (30)

Table S9. The ratio of the integrated areas for *v*(O-D) of Si-OD (2350-2800 cm^{-1}) to those for *v*(O-H) of Si-OH (3300-3750 cm^{-1}) in IR spectra of dehydrated TS-1 zeolites.

Entry	Catalyst	A_1(3300-3750 cm^{-1})	A_2(2350-2800 cm^{-1})	A_2/A_1(*10^{-2})
1	S-1	158.397	0	0
2	S-1-D	45.711	89.173	195.1
3	S-1-D-TBHP	99.128	39.713	40.0
4	TS-1	113.630	0	0
5	TS-1-D	42.685	64.334	150.7
6	TS-1-D-H_2O	210.858	5.299	2.5
7	TS-1-D-MeOH	34.379	44.505	129.5
8	TS-1-D-Decane	37.783	52.116	137.9
9	TS-1-D-TBHP	67.589	6.718	9.9
10	TS-1-D-TBHP-MeOH	99.974	4.517	4.5
11	TS-1-D-TBHP-EtOH	82.457	4.230	5.1
12	TS-1-D-TBHP-1-PrOH	62.516	3.707	5.9
13	TS-1-D-TBHP-1-BuOH	58.324	3.537	6.1

Section S5. Structural properties characterizations of TS-1, A-E.

The XRD patterns in Fig. S10A confirm that TS-1, A-E zeolites have the typical MFI structure and contain no impurity of other zeolite phases [49]. All TS-1, A-E samples have mainly micropore and the micropore volumes of TS-1, B-E samples are slightly lower than that of TS-1A (Table S10) due to that the dissolved Si species under alkali conditions block partial porous channels [47]. However, TS-1, A-E catalysts presented an incremental 1-hexene epoxidation activity (Fig. 4C). Generally speaking, the high total surface area and total volume improve catalytic activity. For the slightly changed micropore volumes of TS-1, A-E catalysts, active Ti species should play a bigger role in catalytic performance. All Si/Ti ratios of TS-1, A-E remain at about 75, implying that no serious dissolution of Si species occurred, but ethylamine molecule just selectively dissolves the Si species around Ti sites [47]. The SEM images in Fig. S11 show that all TS-1 samples keep a plate-like particle morphology. The notable bands at –113 ppm and –103 ppm in the ^{29}Si MAS NMR spectra were assigned to the $Si(OSi)_4$ (Q^4) and $Si(OSi)_3OH$ (Q^3) configurations, respectively [53]. The area percentages of the band at –103 ppm among TS-1, A-E samples are almost unchanged (Fig. S10B), suggesting that their hydrophobicity is approximate. In summary, there is no significant distinction in basic structures and physicochemical properties among these five kinds of TS-1 zeolites.

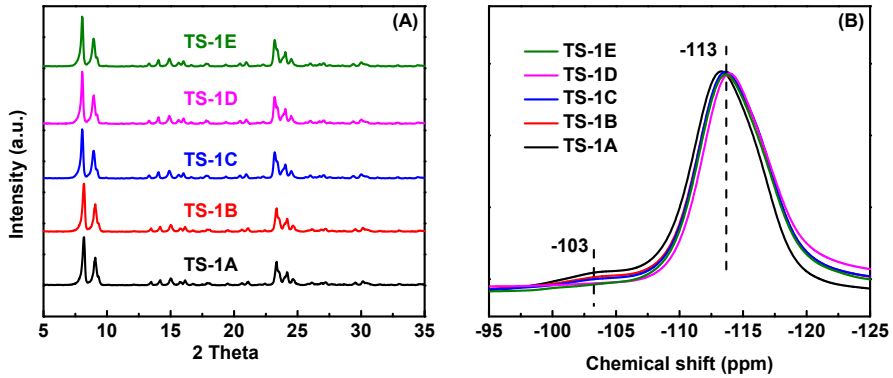

Fig. S10. XRD patterns (A) and ^{29}Si MAS NMR spectra (B) of TS-1, A-E samples.

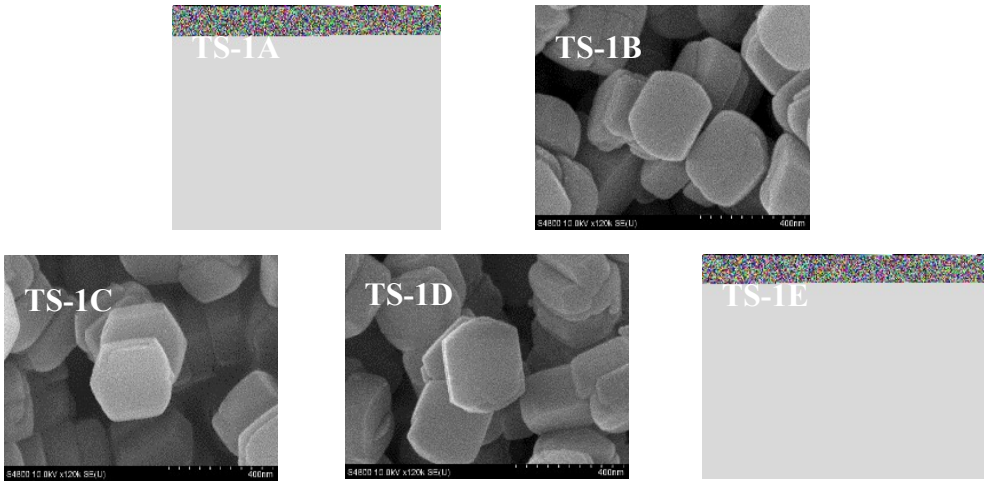

Fig. S11. SEM images of TS-1, A-E samples.

Table S10. Physicochemical properties of various TS-1 zeolites

Entry	Catalyst	S_{micro}[a]	V_{micro}[a]	V_{meso}[a]	Si/Ti[b]
1	TS-1 (TS-1A)	407	0.179	0.102	75
2	TS-1B	382	0.169	0.095	75
3	TS-1C	357	0.158	0.098	75
4	TS-1D	339	0.148	0.082	75
5	TS-1E	350	0.154	0.082	75

[a] Calculated by BET method and t-plot method. S_{micro} ($m^2 \cdot g^{-1}$), V_{micro} ($cm^3 \cdot g^{-1}$), and V_{meso} ($cm^3 \cdot g^{-1}$) stand for microporous surface area, microporous volume, and mesoporous volume, respectively. [b] Detected by ICP.

Table S11. Details of the UV-Vis peak deconvolution of various zeolites from Fig. 3.

Entry	Catalyst	$\Phi_{203}(FWHM_{203})$	$\Phi_{230}(FWHM_{230})$	$\Phi_{270}(FWHM_{270})$
1	TS-1A	84.6 (43)	9.5 (30)	5.9 (47)
2	TS-1B	75.9 (43)	19.7 (34)	4.4 (51)
3	TS-1C	72.7 (39)	22.5 (31)	4.8 (48)
4	TS-1D	63.2 (37)	29.7 (32)	7.1 (48)
5	TS-1E	58.8 (40)	33.5 (34)	7.7 (51)

Φ_x is the ratio of the peak area at x nm to the total area. $\Phi_x = A_x/(A_{203+}A_{230+}A_{270})$. $FWHM_x$ is the full width at half maximum of the peak area at x nm.

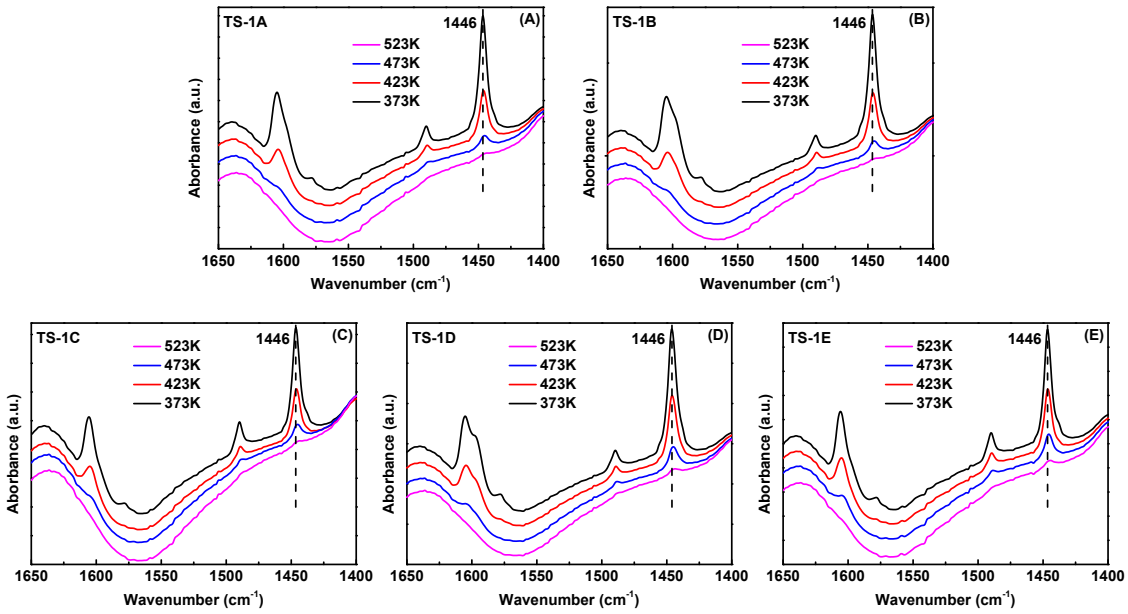

Fig. S12. The FT-IR spectra in the pyridine regions of TS-1, A-E (A-E) at different evacuation temperatures.

Section S6. Comparison of TS-1 and Ti-MWW.

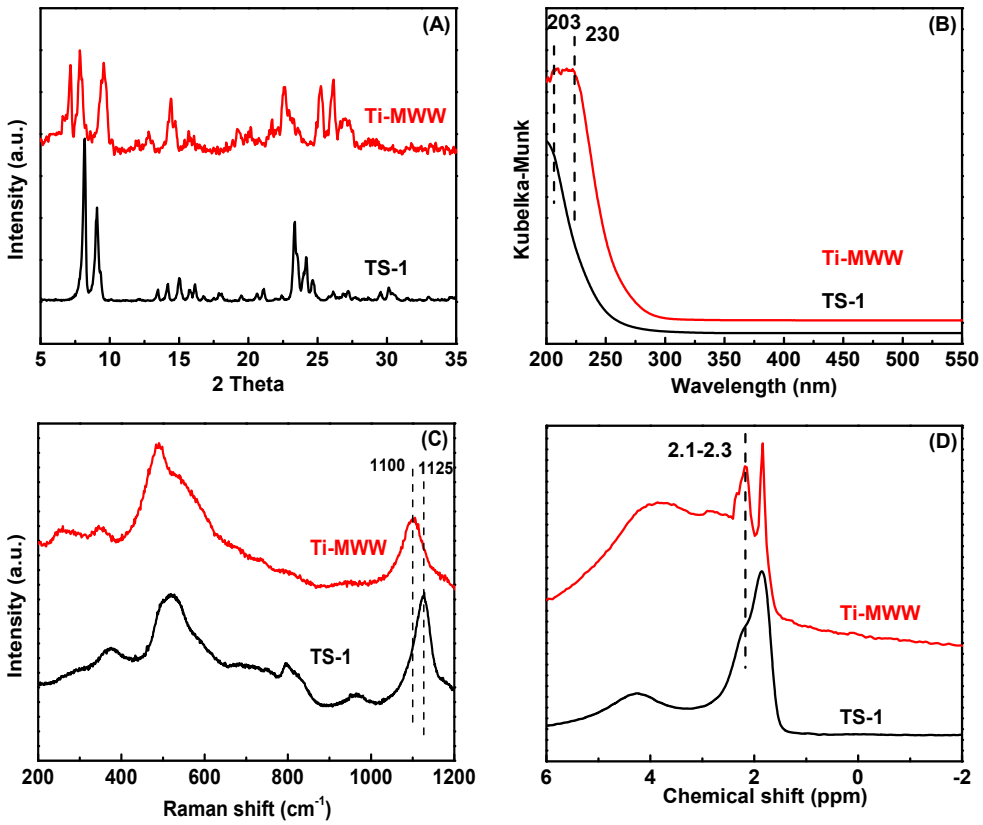

Fig. S13. XRD (A), UV-Vis (B), UV-Raman (C), and ^{1}H MAS NMR (D) spectra of TS-1 and Ti-MWW.

The XRD patterns in Fig. S13A confirm that TS-1 has the typical MFI topological structure, while Ti-MWW has the three-dimensional MWW structure, and they contain no impurity of other zeolite phases. Figure S13B shows the UV-Vis spectra of TS-1 and Ti-MWW. The bands at 203 nm and 230 nm were attributed to the "closed" tetrahedrally coordinated titanium species ($Ti(OSi)_4$) and the "open" tetrahedral titanium ($Ti(OSi)_3OH$) species, respectively [50]. The Ti active site of TS-1 is mainly $Ti(OSi)_4$ species at 203 nm, while the main band at 230 nm of Ti-MWW indicates that it possesses abundant "open" $Ti(OSi)_3OH$ species (Fig. S13B). Figure S13C shows the UV-Raman spectra of TS-1 and Ti-MWW. The band at 1125 cm^{-1} of TS-1 was attributed to the rigid and "closed" $Ti(OSi)_4$ species. The band at 1100 cm^{-1} of Ti-MWW indicates that its Ti coordination environment of "open" $Ti(OSi)_3OH$

species is more flexible [54]. The ^{1}H MAS NMR spectra of the Ti-MWW and TS-1 samples are shown in Fig. S13D. The Ti-MWW sample had more Ti-OH species with a stronger band at 2.1-2.3 ppm than TS-1 [55], further supporting that Ti-MWW possesses abundant "open" $Ti(OSi)_3OH$ species.

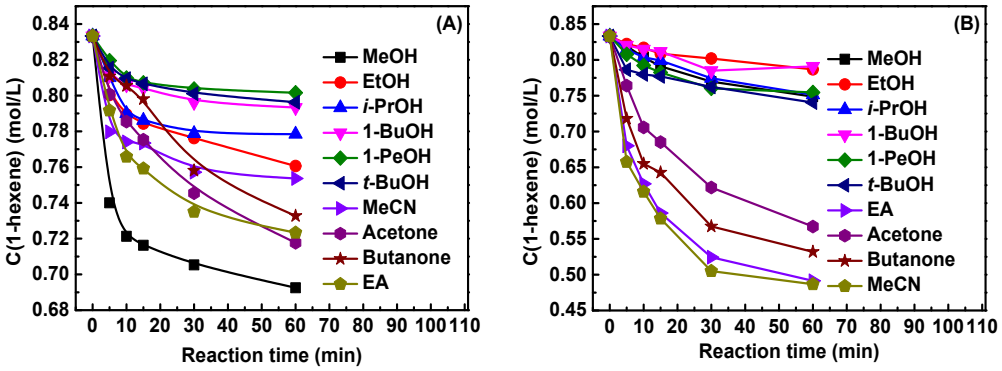

Fig. S14. Effect of reaction time on the epoxidation of 1-hexene over TS-1 (A) and Ti-MWW (B) in various solvents (A). Reaction conditions: catalyst 50 mg, solvent 10 mL, 1-hexene 10 mmol, H_2O_2 (30 wt % aqueous solution) 10 mmol, 333 K, 0 min–60 min.

Note: To explore the source of the difference in catalytic oxidation capacity of different active sites with various solvents, we compared systemically the 1-hexene epoxidation over the two typical titanosilicates (Ti-MWW and TS-1) in various solvents (protic solvent: MeOH, EtOH, *i*-PrOH, 1-BuOH, *t*-BuOH, and 1-PeOH; aprotic solvent: MeCN, Acetone, Butanone, and ethyl acetate (EA)). For avoiding the deactivation of titanosilicates, the initial reaction rates of epoxidation over TS-1 and Ti-MWW were calculated from tangential slopes at reaction time (t) = 0 using exponential curve fitting [56] from the data in Fig. S14, and it was plotted against proton donation ability (acidity) and nucleophilic ability (DN) of solvents in Fig. 6.

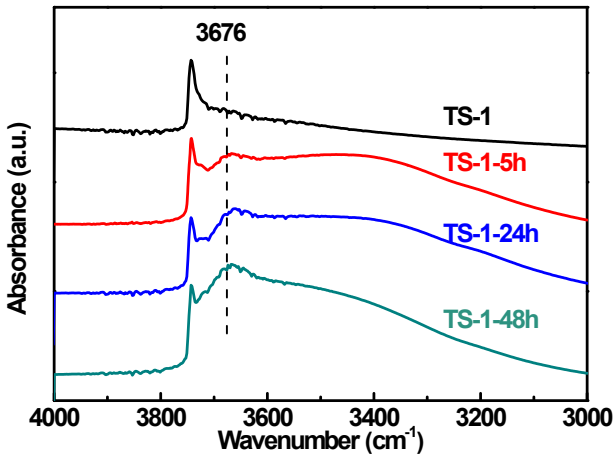

Fig. S15. IR spectra in the hydroxyl stretching evacuated at 723 K in the range of 3000-4000 cm^{-1} of various TS-1 samples.

Note: TS-1-xh zeolites (x represents the treatment time) were prepared through ammonium hydroxide and H_2O_2 treatment of TS-1 to simulate the ammoximation condition. The aqueous solutions have the molar compositions of 1 SiO_2/50 H_2O/2.8 NH_3/1.8 H_2O_2, which were stirred at 343 K for 5, 24, and 48 h. Then TS-1-xh samples were acquired by filtration and subsequently drying, and calcining.

REFERENCES

1. Fan, W.; Wu, P.; Tatsumi, T., *J. Catal.* **2008,** *256* (1), 62-73.
2. Wu, P.; Tatsumi, T., *J. Phys. Chem. B* **2002,** *106* (4), 748-753.
3. Wu, P.; Tatsumi, T., *Chem. Commun.* **2001,** (10), 897-898.
4. Wang, L.; Liu, Y.; Xie, W.; Zhang, H.; Wu, H.; Jiang, Y.; He, M.; Wu, P., *J. Catal.* **2007,** *246* (1), 205-214.
5. Wu, P.; Nuntasri, D.; Liu, Y.; Wu, H.; Jiang, Y.; Fan, W.; He, M.; Tatsumi, T., *Catal. Today* **2006,** *117* (1-3), 199-205.
6. Wu, P.; Liu, Y.; He, M.; Tatsumi, T., *J. Catal.* **2004,** *228* (1), 183-191.
7. Wu, P.; Tatsumi, T., *J. Catal.* **2003,** *214* (2), 317-326.
8. Corma, A.; Esteve, P.; Mart´ınez, A., *J. Catal.* **1996,** *161* (1), 11-19.
9. Fan, W.; Kubota, Y.; Tatsumi, T., *ChemSusChem* **2008,** *1* (3), 175-178.
10. Wu, H.; Liu, Y.; Wang, L.; Zhang, H.; He, M.; Wu, P., *App. Catal. A: Gen.* **2007,** *320*, 173-180.
11. Wu, H.; Wang, L.; Zhang, H.; Liu, Y.; Wu, P.; He, M., *Green Chem.* **2006,** *8* (1), 78-81.
12. Wei; Xie; Yuting; Zheng; Song; Zhao; Junxia; Yang; Yueming; Liu, *Catal. Today* **2010,** *157* (1-4), 114-118.
13. Roffia, P.; Leofanti, G.; Cesana, A.; Mantegazza, M.; Padovan, M.; Petrini, G.; Tonti, S.; Gervasutti, P., *Stud. Surf. Sci. Catal.* **1990,** *55*, 43-52.
14. Song, F.; Liu, Y.; Wu, H.; He, M.; Wu, P.; Tatsumi, T., *J. Catal.* **2006,** *237* (2), 359-367.
15. Wu, C.; Wang, Y.; Mi, Z.; Li, X.; Wei, W.; Min, E.; Han, S.; Fei, H.; Fu, S., *React. Kinet. Catal. Lett.* **2002,** *77* (1), 73-81.
16. Thangaraj, A., Puthoor, L., and Sivasanker, S., *Ind., J. Chem.* **1994,** *33A*, 255-258.
17. Tuel, A.; Moussa-Khouzami, S.; Taarit, Y. B.; Naccache, C., *J. Mol. Catal.* **1991,** *68* (1), 45-52.
18. G. Clerici, M., *Appl. Catal.* **1991,** *68* (1), 249-261.
19. Kon, Y.; Yokoi, T.; Yoshioka, M.; Uesaka, Y.; Kujira, H.; Sato, K.; Tatsumi, T., *Tetrahedron Lett.* **2013,** *54* (36), 4918-4921.
20. Hulea, V.; Fajula, F.; Bousquet, J., *J. Catal.* **2001,** *198* (2), 179-186.
21. Xia, C.; Shu, X.; Long, J.; Yi, Z.; Xu, H.; Zhu, B.; Gao, F.; Min, L.; Dai, Z.; Zou, X., *Chin. J. Catal.* **2015,** *36* (006), 845-854.
22. Bhaumik, A.; Kumar, P.; Kumar, R., *Catal. Lett.* **1996,** *40* (1), 47-50.
23. Clerici, M. G.; Ingallina, P., *J. Catal.* **1993,** *140* (1), 71-83.
24. Vayssilov, G. N.; van Santen, R. A., *J. Catal.* **1998,** *175* (2), 170-174.
25. Wells, D. H.; Delgass, W. N.; Thomson, K. T., *J. Am. Chem. Soc.* **2004,** *126* (9), 2956-2962.
26. M. Taramasso; G. Perego; B. Notari Preparation of porous crystalline synthetic material comprised of silicon and titanium oxides. 1983.
27. Ramachandran, C. E.; Zhao, Q.; Zikanova, A.; Kocirik, M.; Broadbelt, L. J.; Snurr, R. Q., *Catal. Commun.* **2006,** *7* (12), 936-940.
28. Langhendries, G.; De Vos, D. E.; Baron, G. V.; Jacobs, P. A., *Journal of Catalysis* **1999,** *187* (2), 453-463.
29. Ramachandran, C. E.; Du, H.; Kim, Y. J.; Kung, M. C.; Snurr, R. Q.; Broadbelt, L. J.,

Journal of Catalysis **2008,** *253* (1), 148-158.
30. Jiao, W.; He, Y.; Li, J.; Wang, J.; Tatsumi, T.; Fan, W., *Applied Catalysis A: General* **2015,** *491*, 78-85.
31. Yin, J.; Jin, X.; Xu, H.; Guan, Y.; Peng, R.; Chen, L.; Jiang, J.; Wu, P., *Chinese Journal of Catalysis* **2021,** *42* (9), 1561-1575.
32. Drago, R. S.; Dias, S. C.; McGilvray, J. M.; Mateus, A. L. M. L., *J. Phys. Chem. B* **1998,** *102* (9), 1508-1514.
33. Na, K.; Jo, C.; Kim, J.; Ahn, W.-S.; Ryoo, R., *ACS. Catal.* **2011,** *1* (8), 901-907.
34. Wang, L.; Liu, Y.; Xie, W.; Wu, H.; Li, X.; He, M.; Wu, P., *J. Phys. Chem. C* **2008,** *112* (15), 6132-6138.
35. Li, M.; Wang, Y.; Wu, Y.; Wang, M.; Zhou, D., *Catal. Sci. Technol.* **2017,** *7* (18), 4105-4114.
36. Russo, V.; Tesser, R.; Santacesaria, E.; Di Serio, M., *Ind. Eng. Chem. Res.* **2014,** *53* (15), 6274-6287.
37. Nie, X.; Ji, X.; Chen, Y.; Guo, X.; Song, C., *Mol. Catal.* **2017,** *441*, 150-167.
38. Sever, R. R.; Root, T. W., *J. Phys. Chem. B* **2003,** *107* (17), 4080-4089.
39. Nie, X.; Ren, X.; Ji, X.; Chen, Y.; Janik, M. J.; Guo, X.; Song, C., *J. Phys. Chem. B* **2019,** *123* (34), 7410-7423.
40. Bregante, D. T.; Johnson, A. M.; Patel, A. Y.; Ayla, E. Z.; Cordon, M. J.; Bukowski, B. C.; Greeley, J.; Gounder, R.; Flaherty, D. W., *J. Am. Chem. Soc.* **2019,** *141* (18), 7302-7319.
41. Bellussi, G.; Carati, A.; Clerici, M. G.; Maddinelli, G.; Millini, R., *J. Catal.* **1992,** *133* (1), 220-230.
42. Yu, Y.; Tang, Z.; Wang, J.; Wang, R.; Chen, Z.; Liu, H.; Shen, K.; Huang, X.; Liu, Y.; He, M., *Journal of Catalysis* **2020,** *381*, 96-107.
43. Gawley, R. E., *Tetrahedron Lett.* **1999,** *40* (23), 4297-4300.
44. Wells, D. H., Jr.; Joshi, A. M.; Delgass, W. N.; Thomson, K. T., *J. Phys. Chem. B* **2006,** *110* (30), 14627-14639.
45. Sinclair, P. E.; Catlow, C. R. A., *J. Phys. Chem. B* **1999,** *103* (7), 1084-1095.
46. Wang, L.; Xiong, G.; Su, J.; Li, P.; Guo, H., *J. Phys. Chem. C* **2012,** *116* (16), 9122-9131.
47. Wu, L.; Tang, Z.; Yu, Y.; Yao, X.; Liu, W.; Li, L.; Yan, B.; Liu, Y.; He, M., *Chem. Commun.* **2018,** *54* (49), 6384-6387.
48. Chen, Z.; Zhang, L.; Yu, Y.; Liu, D.; Fang, N.; Liu, Y.; He, M., *Microporous Mesoporous Mater.* **2022,** *332*, 111715.
49. Wu, P.; Tatsumi, T.; Komatsu, T.; Yashima, T., *J. Phys. Chem. B* **2001,** *105* (15), 2897-2905.
50. Ratnasamy, P.; Srinivas, D.; Knozinger, H., *Adv. Catal.* **2004,** *48* (50), 1-169.
51. Fang, X.; Wang, Q.; Zheng, A.; Liu, Y.; Lin, L.; Wu, H.; Deng, F.; He, M.; Wu, P., *Phys. Chem. Chem. Phys.* **2013,** *15* (14), 4930-4938.
52. Fang, X.; Wang, Q.; Zheng, A.; Liu, Y.; Wang, Y.; Deng, X.; Wu, H.; Deng, F.; He, M.; Wu, P., *Catal. Sci. Technol.* **2012,** *2* (12), 2433-2435.
53. Lu, X.; Zhou, W.-J.; Guan, Y.; Liebens, A.; Wu, P., *Catal. Sci. Technol.* **2017,** *7* (12), 2624-2631.
54. Fan, F.; Feng, Z.; Li, C., *Acc. Chem. Res.* **2010,** *43* (3), 378-387.
55. Zhuang, J.; Yan, Z.; Liu, X.; Liu, X.; Han, X.; Bao, X.; Mueller, U., *Catal. Lett.* **2002,** *83* (1), 87-91.

56. Shin, S. B.; Chadwick, D., *Ind. Eng. Chem. Res.* **2010,** *49*, 8125-8134.